Carpathian Journal of Earth and Environmental Sciences, February 2026, Vol. 21, No. 1, p. 141 – 154; DOI:10.26471/cjees/2026/021/359

PLUVIAL FLOOD HAZARD ASSESSMENT IN THE NITRA RIVER BASIN, SLOVAKIA

Matej VOJTEK[1,2*], Petra HAČKOVÁ[3], Petra MELIŠKOVÁ[1], Anna BORSÍKOVÁ[2], Zuzana JAKABOVÁ[3] & Jana VOJTEKOVÁ[1]

[1]Department of Geography, Geoinformatics and Regional Development, Faculty of Natural Sciences and Informatics, Constantine the Philosopher University in Nitra, Trieda A. Hlinku 1, 949 01 Nitra, Slovakia; mvojtek@ukf.sk, jvojtekova@ukf.sk

[2]Institute of Geography, Slovak Academy of Sciences, Štefánikova 49, 814 73 Bratislava, Slovakia; matej.vojtek@savba.sk, anna.borsikova@savba.sk

[3]Department of Ecology and Environmental Science, Faculty of Natural Sciences and Informatics, Constantine the Philosopher University in Nitra, Trieda A. Hlinku 1, 949 01 Nitra, Slovakia; petra.hackova@ukf.sk, zuzana.jakabova@ukf.sk

**Corresponding author: mvojtek@ukf.sk*

Abstract: The aim of this study is to assess pluvial flood hazard in the Nitra River Basin, which is located in western Slovakia. Four physical-geographical indicators and land use/land cover were processed using geographic information systems (GIS) and high-resolution spatial data. Specifically, these indicators include morphometric properties of terrain (topographic wetness index, sediment transport index, and curvature), infiltration potential of soils (soil texture), lithological conditions, and land use/land cover. The original indicators were processed to 1 m spatial resolution to match the airborne laser scanned (LiDAR) DEM used. Subsequently, categorical indicators were reclassified based on the potential of individual indicator classes for pluvial flooding while the quantitative indicators were rescaled to continuous scale from 1 to 5. The reclassified/rescaled indicators were equally weighted and linearly combined in order to calculate the pluvial flood hazard index (PFHI), which allows spatial distribution of the different flood hazard classes in the Nitra River Basin. Based on the resulting map of PFHI, the basin was divided into five hazard classes with the following share on the basin area: very high (2.58%), high (31.73%), moderate (39.14%), low (18.9%), and very low (7.89%). The results can be useful for Preliminary Flood Risk Assessment in Slovakia, as pluvial flooding has evolved of the same importance as fluvial floods.

Keywords: pluvial flooding, indicators, geographic information systems, Nitra River Basin, Slovakia

1. INTRODUCTION

Pluvial floods represent a dangerous natural hazard caused by short-duration but extremely intense rainfall that exceeds the infiltration capacity of the soil and the local drainage capability. Unlike riverine floods, they occur independently of watercourses and can affect different areas, from open landscape to densely urbanized areas (Smith & Ward, 1998). In urban areas, the risk is further amplified due to high proportions of impervious surfaces, limited retention capacity, and capacity constraints of sewer networks (Cea et al., 2025).

The observed increase in the frequency of intense rainfall events in recent decades corresponds with trends identified in global climate models, which indicate an increase in short-duration rainfall extremes due to atmospheric warming (IPCC, 2021; Rosenzweig et al., 2018). These phenomena pose significant challenges for flood risk management, as traditional methods developed for assessing floods often fail to capture the highly localized nature of surface runoff (Vojtek & Vojteková, 2018; Vojtek et al., 2023a). Research therefore emphasizes a more detailed understanding of terrain processes and spatial factors influencing runoff generation and concentration (Bartlett et al., 2025).

Different approaches can be used for pluvial flood hazard mapping and assessment. One of them is the physically-based approach represented by

rainfall-runoff and hydraulic models. The advantage of this approach is that it can provide high-precision results. On the other hand, it is suitable for local-scale study areas due to high demands for input data, having also long computational times (Teng et al., 2017; Mudashiru et al., 2021; Welten et al., 2024). The other approaches focus on determining spatial flood hazard using different groups of methods. Multi-criteria methods, such as analytical hierarchical process, weighted linear combination, or analytical network process are based on subjective ranking and weighting of indicators to derive the flood hazard index (Santos et al., 2019; Toosi et al., 2019; Vojtek et al., 2021). The group of bivariate and multivariate methods is considered more objective, as it relies on statistical methods (Costache, 2019). The group of machine or deep learning methods has been widely used in recent years to classify the spatial flood hazard based on training various machine/deep learning algorithms on mostly physical-geographical predictors and flood inventory data (Costache et al., 2020; Bentivoglio et al., 2022; Vojtek et al., 2023b).

In the context of all groups of methods, geographic information systems (GIS) play a key role in mapping, modeling, and visualizing pluvial flood hazards. GIS enables the integration of diverse spatial data layers, like digital elevation models, land use/land cover data, soils, or lithology, into spatial analyses that identify potential accumulation zones and critical areas (Zoppou, 2001; Maidment, 2002). Research indicates that the combination of physical-geographical and land use/land cover data is essential for understanding the complex nature of pluvial flooding (Dau et al., 2024).

Input data used for deriving the pluvial flood hazard index may vary. In general, various physical-geographical indicators, characterizing mainly morphometric properties of terrain, infiltration capabilities of soils or rocks, or interception of vegetation, are combined with land use/land cover indicator or other socio-economic indicators (Krvavica et al., 2023; Allegri et al., 2024). Combining datasets introduces constraints with spatial resolutions or map scales of source data. This possible limitation can bias spatial flood hazard mapping and distort the relative importance of influencing factors (Saha et al., 2021; Yu et al., 2025). In particular, the digital elevation model (DEM) is one of the most important data sources for spatial flood hazard mapping. Coarse DEMs fail to capture small-scale features in the terrain. This can lead to errors in slope, flow direction, accumulation, and other morphometric factors, ultimately limiting the precision and applicability of spatial flood hazard assessments (Jiang et al., 2022). Therefore, the spatial modeling of pluvial flood hazard should be based on high-resolution data, like those obtained from aerial laser scanning or aerial imagery (Blöschl et al., 2024).

Despite the fact that pluvial flooding has been less researched so far as the fluvial flooding, pluvial flooding can pose economic or societal risks comparable to those of fluvial flooding, especially, in urban environments (Rözer et al., 2021; Mediero et al., 2022; Tanaka et al., 2020). Due to climate change processes, anticipated increase in the frequency and intensity of extreme rainfall, and spread of impervious surfaces, the pluvial flood hazard may increase in the future. Therefore, greater effort should be placed to study also this type of flood (Papalexiou & Montanari, 2019).

The aim of this study is to analyze pluvial flood hazard using GIS tools and weighted linear combination, which enable to identify the most susceptible locations, and evaluate the factors influencing runoff conditions in the study area.

2. MATERIALS AND METHODS

2.1. Study area

The Nitra River is located in western Slovakia (Figure 1). The total length of the Nitra River is 167 km. The studied area of the Nitra River Basin covers 4,488 km², forming 28% of the Váh River Basin.

The geographical coordinates of the studied area are as follows: northernmost point (48°58′N, 18°34′E), southernmost point (47°57′N, 18°08′E), westernmost point (48°09′N, 17°52′E), and easternmost point (48°44′N, 18°49′E).

Based on the geomorphological classification by Mazúr & Lukniš (1986), the studied area belongs to these geomorphological units: Podunajská rovina plain, Podunajská pahorkatina hills, Tribeč mountain, Strážovské vrchy mountain, Hornonitrianska kotlina mountain, Žiar mountain, Považský Inovec mountain, Vtáčnik mountain, and Pohronský Inovec mountain. The highest point has an elevation of 1,346 m a. s. l. and it is located on the eastern border of the studied area in the Vtáčnik mountain range. The lowest point is found at the Nitra River mouth (108 m a. s. l.).

According to the climate region classification of Slovakia by Lapin et al. (2002), the Nitra River Basin is located in three main climate regions. The warm climate region is mainly found in the lowland part of the basin, particularly in the Podunajská nížina lowland and at the foothills of Tribeč mountain. This region is characterized by mild winters, long and warm summers, and relatively low precipitation totals. The average annual temperature exceeds 9 °C, and the annual precipitation ranges from 500 to 700

mm. The moderately warm climate region includes Považský Inovec, Tribeč, Strážovské vrchy mountains, and parts of the Nitrianska pahorkatina hills. Temperatures here are slightly lower than in the lowlands, with an average annual temperature between 6 and 9 °C, and annual precipitation between 600 and 900 mm. The cold climate region occurs at higher elevations, primarily in mountain ranges such as Strážovské vrchy and Považský Inovec mountains. Average annual temperatures are below 6 °C, and annual precipitation can exceed 1,000 mm. This region is characterized by cold and humid conditions, with frequent snowfall during winter months.

The Nitra River originates in the Malá Fatra mountain range, below the Reváň peak (1,205 m a. s. l.) at an elevation of approximately 770 m a. s. l., and forms a left-hand tributary of the Váh River. The left-hand tributaries of the Nitra River include, for example, the Handlovka, Žitava, and Vyčoma rivers, while the right-hand tributaries include the Bebrava, Radošinka, Nitrica, and Dlhý kanál rivers. The Nitra River flows through major towns, such as Prievidza, Topoľčany, Nitra, and Nové Zámky.

As for the administrative division of Slovakia, the studied area belongs to the Western Slovakia (NUTS II), the Trenčín Region (NUTS III), the Nitra Region (NUTS III), the Banská Bystrica Region (NUTS III), and the Trnava Region (NUTS III).

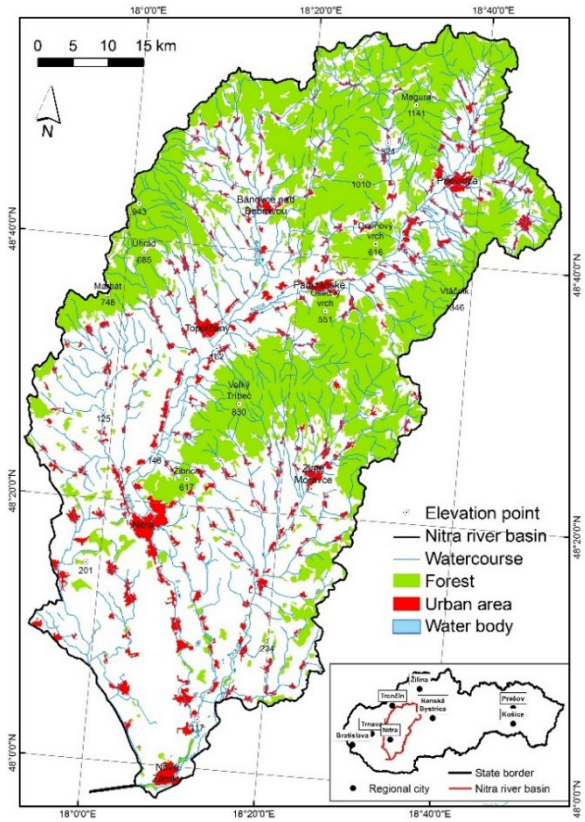

Figure 1. Study area of Nitra River Basin in Slovakia.

2.2. Data processing

In this subsection, we focus on the data and methods used to develop indicators for assessing pluvial flood hazard in the Nitra River Basin. Specifically, it was the topographic wetness index (TWI), sediment transport index (STI), curvature, lithological rock types, soil texture types, and land use/land cover (LULC). These factors influence the landscape's ability to retain water, regulate runoff, and identify areas at risk of pluvial flooding. The indicators used were processed and visualized in ArcGIS 10.2.2.

The slope map of the Nitra River basin was created using a digital elevation model (DEM) (DMR5.0) with a resolution of 1 m, derived from airborne laser scanning (LiDAR). This DEM was obtained from the Geodetic and Cartographic Institute. The slope classification was carried out according to the methodology of Demek (1972). Curvature map was generated from the LiDAR DEM using ArcGIS 10.2.2.

In a similar way, i.e. based on the DEM and the flow direction raster, a flow accumulation map was generated. To calculate the synthetic TWI indicator, we used Equation (1) that is a function of terrain slope and flow accumulation (Beven & Kirkby, 1979):

$$TWI = Ln\left(\frac{A}{tan\beta}\right) \quad (1)$$

where A is the upslope contributing area draining through a given point per unit contour length, and $tan\beta$ is the slope gradient expressed in radians.

The STI was calculated based on DEM and Equation (2) derived by Moore & Burch (1986):

$$STI = \left(\frac{A_S}{22.13}\right)^m \times \left(\frac{sin\beta}{0.0896}\right)^n \quad (2)$$

where A_s is the specific catchment area (or unit contributing area), which represents the upslope contributing area per unit contour length, β is the local slope gradient in degrees, m and n are empirical exponents with values m=0.6 and n=1.3.

The lithology map, which represents individual types of rocks, was processed based on the vector layer of the Engineering-geological Zoning Map of the Slovak Republic at a scale of 1:50,000, available on the web portal of the State Geological Institute of Dionýz Štúr (Vojtek et al., 2022). Rock permeability was defined to individual types of rocks according to Hrnčiarová (1993).

The soil texture map was created based on vector layers of the Bonited Soil-ecological Units (BPEJ), which were obtained from the Soil Science and Conservation Research Institute in Bratislava, and forest soil units acquired from the National Forest

Centre in Zvolen.

The land use/land cover map was prepared based on the Basic Data Base for Geographic Information System (ZBGIS) from 2023, which was provided by the Geodetic and Cartographic Institute.

2.3. Calculation of pluvial flood hazard index

In the case of rock permeability, soil types, and land use/land cover, we reclassified these indicators into five classes according to their potential for the occurrence of pluvial flooding. Class 5 represents the highest potential, while class 1 represents the lowest potential to pluvial flooding (Table 1). As for the TWI and STI indicators, they were rescaled to a continuous range of values from 1 to 5.

Table 1. Reclassification of indicators with respect to the potential of their classes to pluvial flood occurrence.

Reclassified indicator	Class	Reclassification (1 – lowest potential for pluvial flooding, 5 – highest potentital for pluvial flooding)
Curvature (accumulation potential)	Convex	1
	Linear	3
	Concave	5
Lithology (rock permeability)	Very high	1
	High	2
	Moderate	3
	Low	4
	Very low	5
Soil texture (infiltration potential)	Sandy	1
	Sandy-loamy	2
	Loamy-sandy	2
	Loamy	3
	Clayey-loamy	4
	Clayey and clay	5
LULC based on ZBGIS (infiltration potential)	Forest, watercourse, water body	1
	Shrub, orchard, grassland, urban greenery	2
	Vineyard, hop field	3
	Arable land	4
	Built-up area, material/waste dump, road, railway	5

To calculate the pluvial flood hazard index (PFHI), we applied equal weighting of the indicators (Vojtek et al., 2024), i.e. a weight of 1/6 was assigned to each of the six reclassified/rescaled indicators in order to maintain the scale 1–5. Equation (3) was used to calculate the PFHI:

$$PFHI = \sum_j x_j^{'} 1/6 \quad (3)$$

where *PFHI* is the pluvial flood hazard index and *x'j* is the reclassified or rescaled *j*-th indicator.

3. RESULTS AND DISCUSSION

3.1. Pluvial flood indicators

3.1.1. TWI

The slope of the terrain represents one of the key physical-geographic factors influencing the hydrological regime of the basin. The steepness and orientation of slopes significantly determine the rate of surface runoff and thus the potential for pluvial flood formation. Areas with steeper slopes are more prone to rapid surface runoff, whereas gently sloping and flat parts of the basin provide greater potential for water accumulation into the soil.

For a more comprehensive assessment of pluvial flood hazard, it is necessary to consider additional factors such as flow accumulation and the Topographic Wetness Index (TWI). These datasets allow the identification of locations with a higher potential for water concentration and long-term saturation, thereby improving the precision in identifying areas at increased risk of pluvial flood occurrence (Vojtek et al., 2024).

The slope map (Figure 2) illustrates the variation in slope steepness within the Nitra River Basin. The steepest slopes, ranging from 35 to 88°, cover only 0.02% of the basin total area. These slopes are found predominantly in the northern part of the basin, especially in the Strážovské vrchy, Malá Magura, and Žiar mountain ranges. Areas with slopes between 15 and 35° are situated adjacent to the steepest terrain and account for 12.39% of the basin area. These slopes delineate the western, northern, and eastern margins of the basin and are located in the areas hills. Terrain with slopes between 5 and 15° covers 31.17% of the basin areas and is primarily concentrated in the Pohronský Inovec and Tribeč mountain ranges. Areas with slopes from 2 to 5° represent 23.18% of the basin area and are characteristic of gently sloping landscapes located mainly in lowland and hilly areas, where the terrain transitions from uplands to flat areas. Such slopes appear, for example, in the Hornonitrianska kotlina basin, where the landscape gradually descends from the Strážovské vrchy and Vtáčnik mountains into the basin, as well as in the Nitrianska pahorkatina hills in the southern part of the basin, where the relief becomes increasingly subdued. The largest proportion of the basin is represented by flat terrain with slopes between 0° and 2°, covering 33.23% of the total basin area. This relief is mainly situated in the lower part of the basin, where the Nitra River flows through the wide Nitra floodplain,

characterized by sediment accumulation and minimal slopes, which increases the risk of water accumulation during intense rainfall.

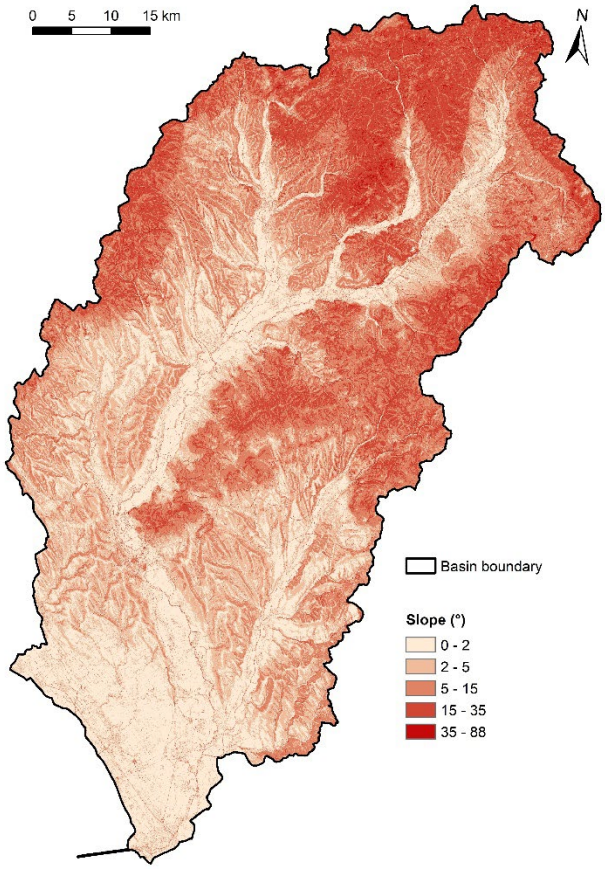

Figure 2. Slope in the Nitra River Basin.

Flow accumulation (Figure 3) represents another crucial indicator for evaluating pluvial flood hazard. The highest flow accumulation values in the basin occur mainly in areas with low slopes, valleys and river channels, promoting water accumulation. These regions are found especially in the lower parts of the basin, notably in the Podunajská nížina lowland, where the Nitra River flows through a wide, flat landscape. Here, the minimal slope facilitates substantial water accumulation, as slow-moving flows do not ensure rapid drainage of rainwater. Such locations are susceptible to retaining large amounts of water, increasing flood risk during intense rainfall. The largest share on the basin area falls within the interval 0–50 pixels, covering 96.27% of the total basin. Share of areas classified in the intervals 500–5000 (1.44%) and 5000–50,000 (1.18%) is substantially lower. Conversely, the lowest share belong to the intervals 50–500 (0.99%) and 50,000–1,651,267 (0.12%). These areas represent larger channels where water converges.

Following the previous analyses of slope and flow accumulation in the Nitra River basin, the TWI (Figure 4) serves as a key synthetic indicator that enhances understanding of moisture conditions across the basin. In the Nitra River basin, the highest TWI values (8.52–23.84 and 6.21–8.52) occur predominantly in areas with low slopes and in locations where the concentration of upslope contributing areas is greatest.

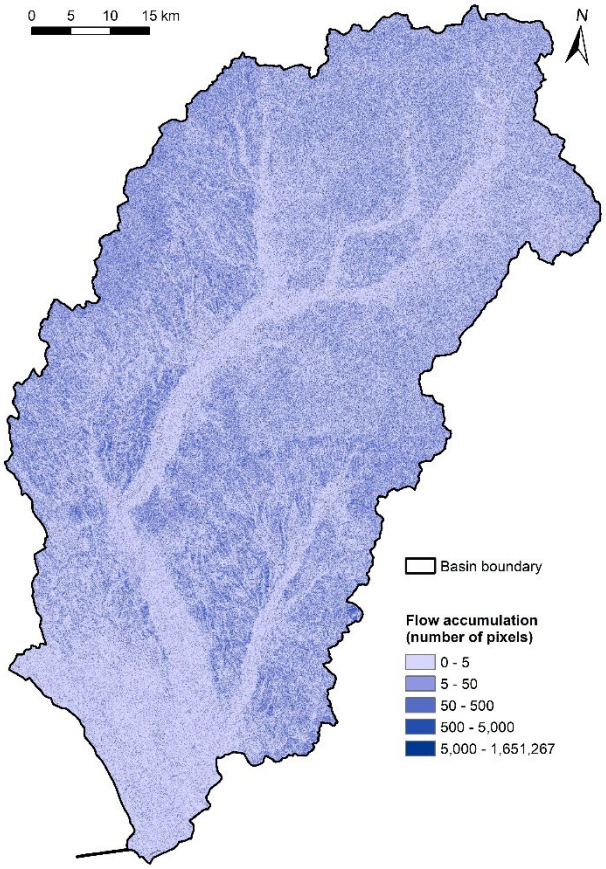

Figure 3. Flow accumulation in the Nitra River Basin.

These areas are typically situated in the lower basin, especially in the Nitra River floodplain and the Hornonitrianska kotlina basin, where the Nitra River flows through wide, relatively flat landscapes. TWI values between 4.44 and 6.21 occupy areas with moderate slopes, where a balanced relationship exists between water accumulation and runoff. These values are typical of the middle basin areas, such as in the Pohronský Inovec and Tribeč mountains. The lowest TWI values in the Nitra River basin occur in areas with the steepest slopes, where rapid water flow prevents accumulation. These include higher and steeper parts of the basin, such as the Strážovské vrchy, Veľký Tribeč, and Malá Magura mountains. These areas correspond to TWI intervals of 2.79–4.44 and (–3.27)–2.79 in the northern and northeastern parts of the basin.

The rescaled TWI values are shown in continuous scale in Figure 5.

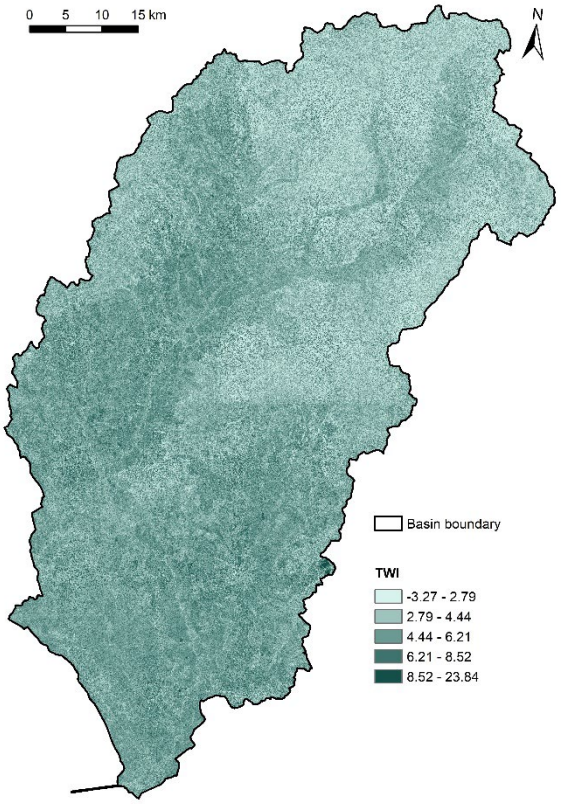

Figure 4. Original TWI in the Nitra River Basin.

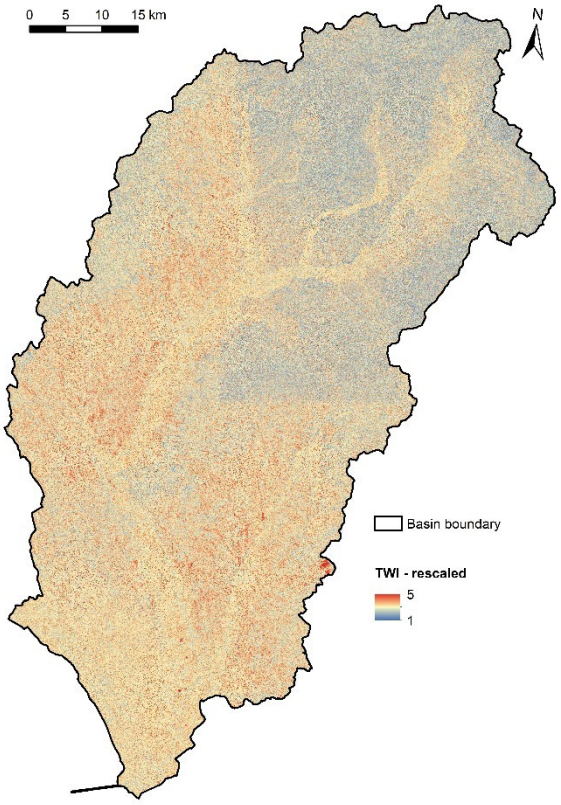

Figure 5. Rescaled TWI in the Nitra River Basin.

3.1.2. STI

STI is another important morphometric indicator, which estimates where erosion is most likely to occur and where sediment is most likely to be transported across a landscape. High STI values indicate high erosion risk, while low values suggest areas where sediment may be deposited.

In the Nitra River basin, the highest STI values occur predominantly in mountainous areas and areas with higher slopes, such as the Strážovské vrchy, Veľký Tribeč, and Malá Magura mountains (Figure 6). The high STI values areas are typically situated in the upper part of the basin, where rapid water flow prevents accumulation. On the other hand, low-lying, low slope, and flat areas, like most of them in the Podunajská pahorkatina hills, have low STI values, where the deposition in dominated.

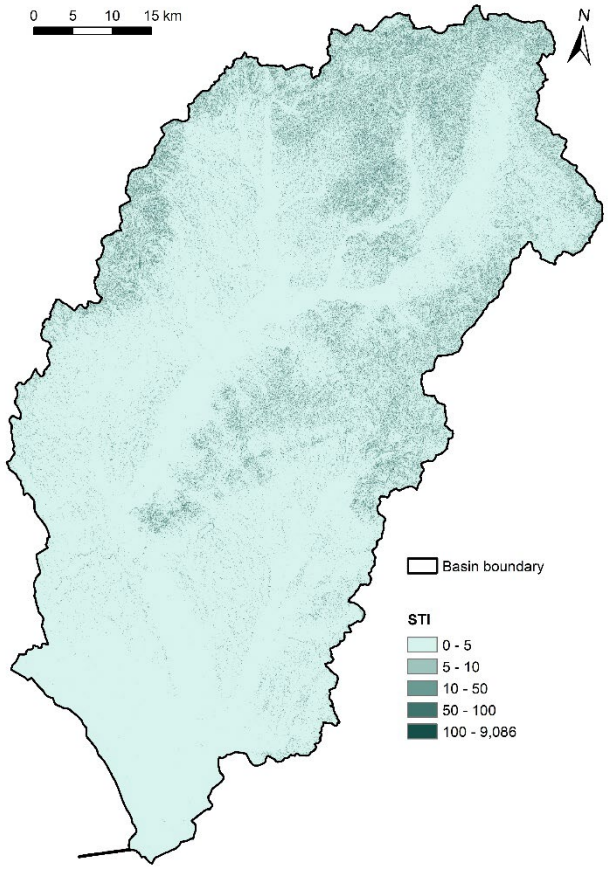

Figure 6. Original STI in the Nitra River Basin.

The rescaled STI map, containing continuous scale, is shown in Figure 7.

3.1.3. Curvature

Curvature is important for runoff as it affects where water accumulates, how quickly it moves, and its erosive potential. Concave slopes can lead to more runoff pooling, while convex slopes can cause water to spread out and decrease runoff.

Most of the relief forms in the Nitra River Basin are concave (44.43%). Similar percentage belongs to convex forms of relief (43.31%). The smallest share

(1.23%) account for linear forms of relief (Figure 8).

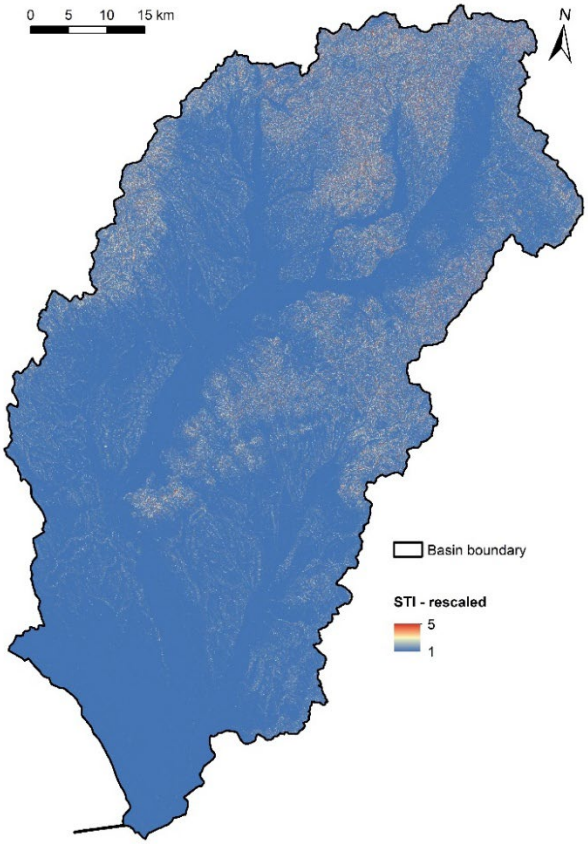

Figure 7. Rescaled STI in the Nitra River Basin.

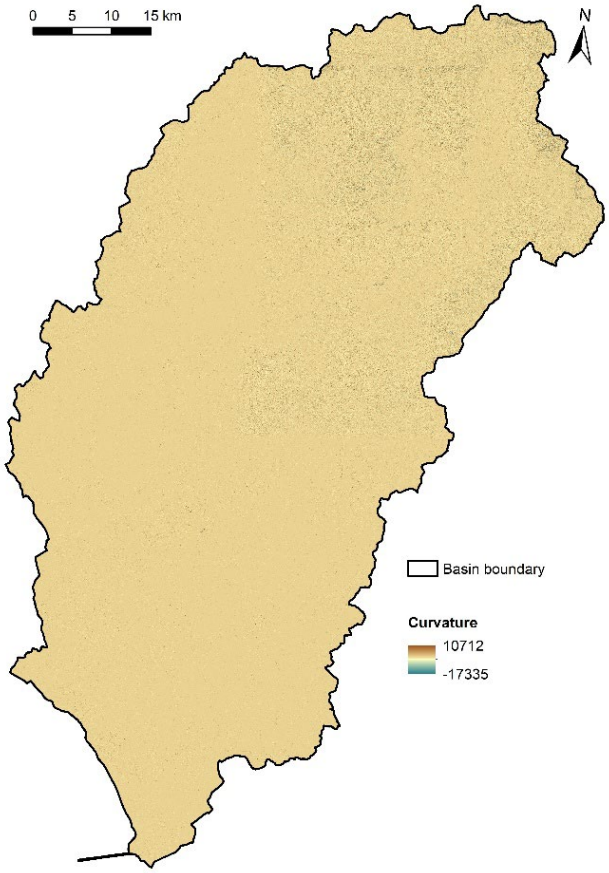

Figure 8. Original curvature in the Nitra River Basin.

The reclassified curvature map to three classes, based on accumulation potential of convex, linear, and concave forms of relief, is shown in Figure 9.

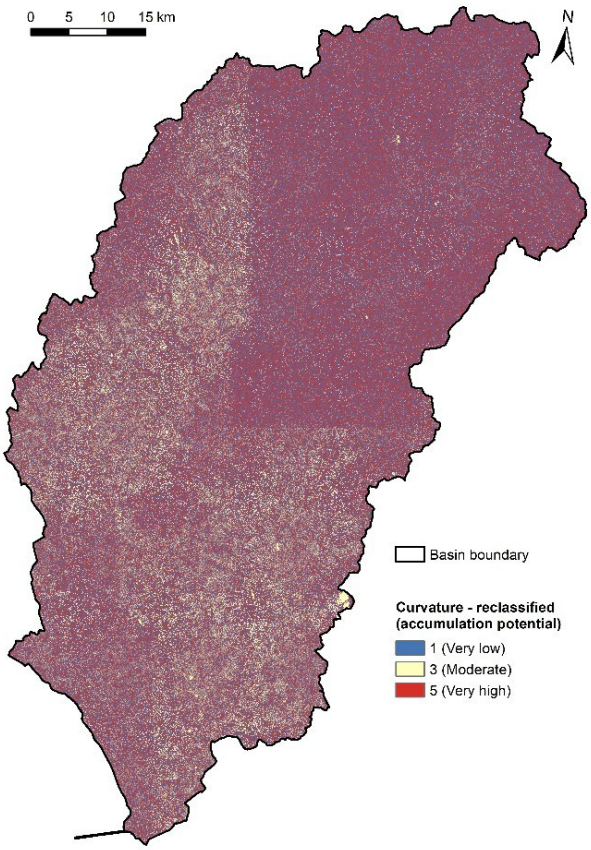

Figure 9. Reclassified curvature in the Nitra River Basin.

3.1.4. Lithology

The lithology plays a significant role in the development and course of pluvial floods, as it influences infiltration, and the landscape's ability to retain rainfall. Differences in rock permeability can substantially contribute to the formation of intense surface runoff during extreme precipitation events. The Nitra River Basin contains a diverse lithological structure that affects the spatial distribution and intensity of flood-related risks.

The distribution of lithological rocks within the Nitra River Basin is shown in Figure 10. The highest share of the basin is formed by the loess region, which covers up to 23.36%. Loess represents a significant sedimentary cover in the basin, especially in its lowland parts. These fine-grained, predominantly silt sediments were formed by aeolian processes. In the context of pluvial floods, loess plays an important role because, once saturated with water, it loses stability and may lead to increased surface runoff, landslides, or mudflows.

Also notably represented is the region of alluvial lowland deposits (10.75%), which includes

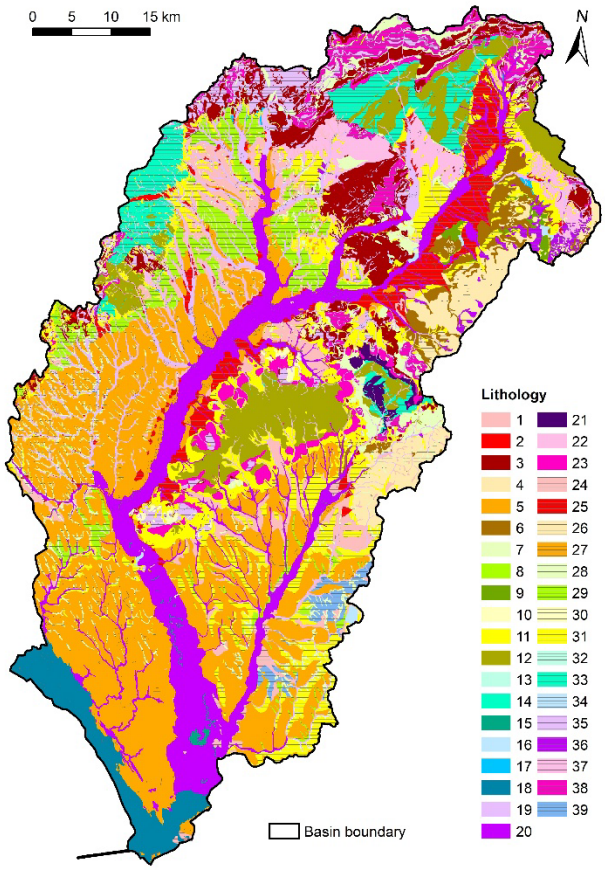

Figure 10. Original lithology in the Nitra River Basin: 1-deluvial sediments, 2-dislocated metamorphosed rocks, 3-dolomite rocks, 4-effusive rocks, 5-aeolian loess, 6-epiclastic rocks, 7-flyschoid rocks, 8-lacustrine and fluvio-lacustrine sediments, 9-fine-grained cohesive sediments, 10-carbonate and clastic rocks, 11-colluvial sediments, 12-magmatic intrusive sediments, 13-metamorphosed carbonates, 14-metamorphosed volcanics, 15-cut-off meanders, 16-waste deposits, 17-neogene conglomeratic sediments, 18-alluvial plain deposits, 19-mountain river deposits, 20-lowland river deposits, 21-low-grade metamorphic rocks, 22-sandstone-conglomerate rocks, 23-sanstone rocks, 24-Pleistocene river terraces, 25-alluvial fans and aprons, 26-pyroclastic rocks, 27-peat bogs, 28-valley sediments, 29-loess sediments, 30-alternating effusive and pyroclastic rocks, 31-alternating fine-grained and gravelly sediments, 32-travertine accumulations, 33-highly metamorphosed rocks, 34-limestone-dolomite rocks, 35-limestone rocks, 36-landslide colluvium, 37-clayey-silty sediments, 38-clayey-limestone rocks, 39-gravelly sediments.

areas with low terrain slopes where the river deposits material and forms a wide floodplain. This region is characterized mainly by Quaternary sediments such as sands, gravels, clays, and silty deposits formed by fluvial processes and is found along the Nitra River. The region of magmatic intrusive rocks (5.93%) contains areas dominated by igneous rocks such as granite. This region is typically located in mountainous parts of the basin, where slopes are steep and the bedrock is less weathered.

Areas where loose slope sediments accumulate due to gravity, precipitation, and surface runoff form the more extensive region of colluvial sediments (5.35%). These sediments consist of a mixture of rock fragments of various sizes, clays, sands, and silts released through weathering and subsequently transported downslope. They occur mainly at the foot of slopes, in valleys, and at the transition between slope and floodplain areas. The region of alternating fine-grained to gravelly sediments covers 4.92%. It includes areas containing sediments of varying grain size, ranging from fine-grained clays and silts to coarse sands and gravels, located mainly in lowland and riverine parts of the basin.

Deluvial sediments cover 4.54%. These deposits consist primarily of clays, sands, gravels, and rock fragments that accumulate at the foot of slopes, in valleys, and on gently inclined terrain. This type of rock includes areas where loose slope deposits accumulate due to gravitational processes and is found mainly in the northwestern part of the basin and around the Tribeč mountain range. The dolomite rocks (4.85%) include areas dominated by dolomite-carbonate rocks with a high content of the mineral dolomite. In the basin, dolomites occur mainly in the Tribeč, Strážovské vrchy, and Považský Inovec mountains. They are characterized by relatively high permeability due to fracture systems and karst cavities that allow rapid infiltration of rainfall into the subsurface. The region of alluvial deposits of mountain streams (4.37%) includes areas where fluvial sediments are present, formed as rivers and streams transport material from higher mountain areas during high flows.

On the other hand, the smallest area of the Nitra River basin is formed by metamorphosed carbonates (0.005%), which includes rocks formed by the metamorphism of original limestones. Very small areas are also occupied by alternating effusive and pyroclastic rocks (0.006%), limestone-dolomite rocks (0.0013%), and lacustrine and fluvio-lacustrine sediments (0.0029%).

The reclassification of lithological rock types into five permeability classes is shown in Figure 11. The largest share on the basin area accounts for highly permeable rocks, covering 60.23% of the basin area. These rocks are located mainly in the southern and central parts of the basin. The second largest category is very high permeability (13.62%), which covers the southeastern and northwestern parts of the basin. Areas with moderate permeability, primarily found in the Vtáčnik and Pohronský Inovec mountains, constitute 12.27% of the basin. In contrast, low permeability (9.33%) is characteristic of the Považský Inovec and

Tribeč mountains. The lowest permeability, covering only 4.55% of the basin, is found mainly in the eastern and northern parts of the basin.

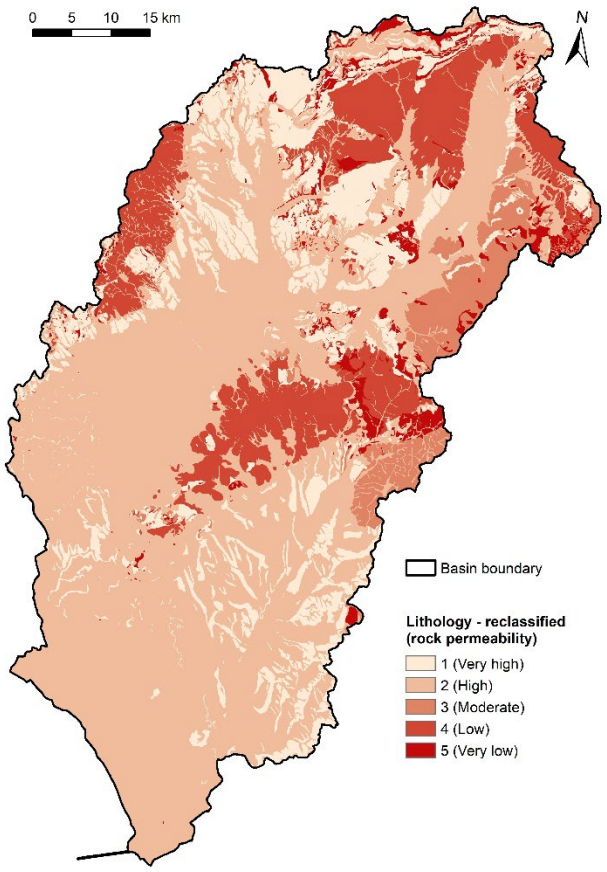

Figure 11. Reclassified lithology in the Nitra River Basin.

3.1.5. Soil texture

The structure of soil texture plays an important role in regulating the water regime and influences the degree of surface runoff during intense rainfall. Their differing physical and permeability properties determine the soil's ability to infiltrate and retain water, thereby directly contributing to the occurrence or mitigation of pluvial floods.

The largest part of the Nitra River basin is formed by loamy soils, which cover up to 56.95% of the basin area (Figure 12). These soils are mainly located in the southern and northern parts of the Podunajská pahorkatina hills, in the northern part of the Hornonitrianska kotlina basin, and in the Strážovské vrchy mountain. Sandy-loamy soils (21.29%) constitute the second most widespread soil texture type and occur primarily in the central part of the Tribeč mountain, as well as in the eastern part of the basin in the Pohronský Inovec, the northwestern part of the Považský Inovec, and the northern part of the Strážovské vrchy mountains. Clayey-loamy soils (15.02%) appear in scattered patches along the Nitra River and are also present on the northern margin of the basin. Loamy-sandy soils (3.89%) have a smaller distribution and are found mainly in the southern part of the basin. In the lower reaches of the Nitra River, clayey soils and clays (1.82%) occur to a limited extent, while sandy soils represent the smallest share (1.02%) and are located in close proximity to loamy-sandy soils.

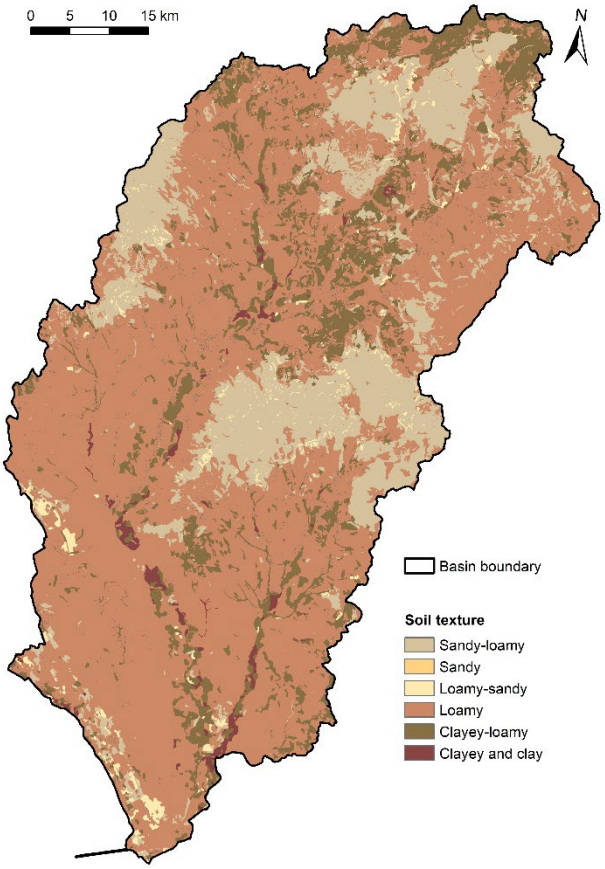

Figure 12. Original soil texture in the Nitra River Basin.

After reclassifying soil texture types into five classes based on their infiltration potential (Figure 13), sandy soils (1.02%) were assigned the highest permeability. They are followed by sandy-loamy and loamy-sandy soils (25.19%), which belong to the second reclassified class. Loamy soils form the largest part of the basin, covering 56.95% of the basin area. Clayey-loamy soils (15.02%) fall into the fourth reclassified class, while clayey soils and clays (1.02%) form the smallest share on the basin area and belong to the last reclassified class with the highest potential for pluvial flooding.

3.1.6. Land use/land cover

Different LULC classes, such as agricultural areas, forest stands, urbanized zones, and water bodies, affect the landscape's ability to absorb precipitation, regulate runoff, and retain water. Some of the LULC classes can increase surface runoff and

thus contribute to more intense pluvial flood events, while others can help mitigate these risks (Vojteková & Vojtek, 2019).

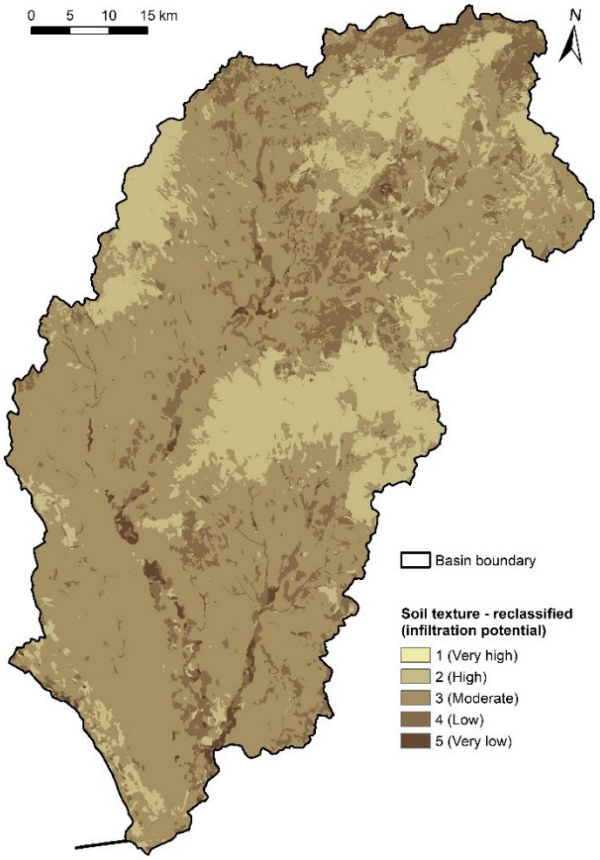

Figure 13. Reclassified soil texture in the Nitra River Basin.

The arable land is the most dominant class, covering 44.31% of the basin (Figure 14). In the Nitra River Basin, it is primarily concentrated in lowland and valley areas, where conditions for agricultural production are most favorable. These areas are mainly situated in the southern and central parts of the basin, where the Nitra River and its tributaries form wide valleys. Arable land covers large portions of the basin, as the conditions for agriculture are advantageous due to fertile fluvial and deluvial sediments.

The second-largest class is forest (36.32%). Forested areas are predominantly found in mountainous and foothill regions, especially in Tribeč, Strážovské vrchy, Považský Inovec, and Vtáčnik mountains. Forest stands play a crucial role in regulating hydrological processes, as they have a high capacity to retain water and reduce the intensity of surface runoff, thereby helping to mitigate the risk of pluvial flooding. Forests promote natural infiltration of precipitation, reducing the amount of water that would otherwise flow directly into rivers and tributaries.

Grassland and shrubs occur mainly in lowland and foothill areas where conditions for these vegetation types are suitable, particularly in the southern and central parts of the basin. Shrub is more common in transitional zones between forests and open areas, as well as on slopes and edges of forest complexes. Together, these two classes account for 4.98% of the basin. Orchards and vineyards (3.99%) are also common and are primarily concentrated in the southern and central parts of the basin, but also scattered in other parts.

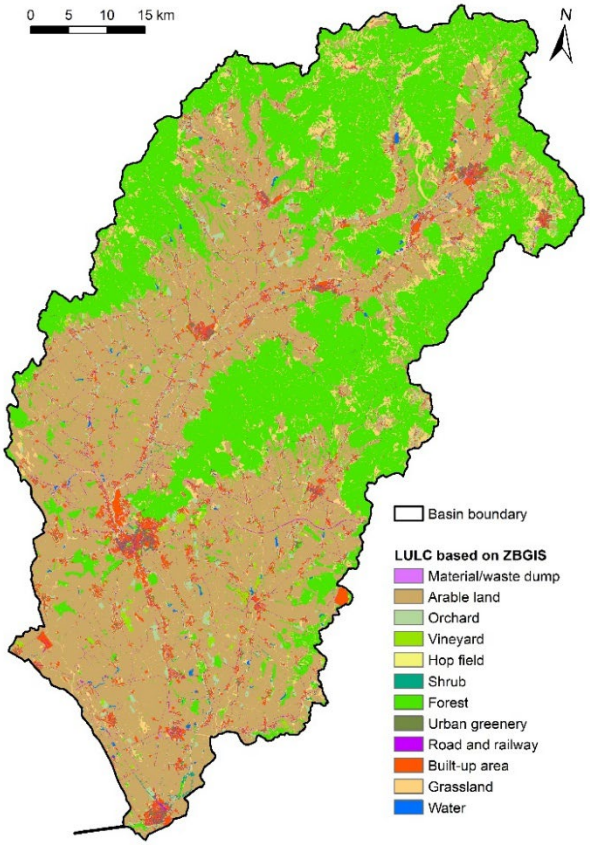

Figure 14. Original LULC in the Nitra River Basin.

The reclassified LULC map based on infiltration potential of individual LULC classes is shown in Figure 15. The largest share belongs to fourth reclassified class, which forms 44.48% of the total basin area. This class is mainly located in the southern and central parts of the basin, where they predominate. The second largest area is represented by first reclassified class, which mainly covers the northern part of the basin, with smaller segments appearing on the eastern and western edges. The second reclassified class accounts for 9.82% of the basin area and is scattered in patches across the basin without a pronounced concentration in specific regions. The smallest representation (5.78%), belongs to fifth reclassified class, while third reclassified class accounts for only 3.02%.

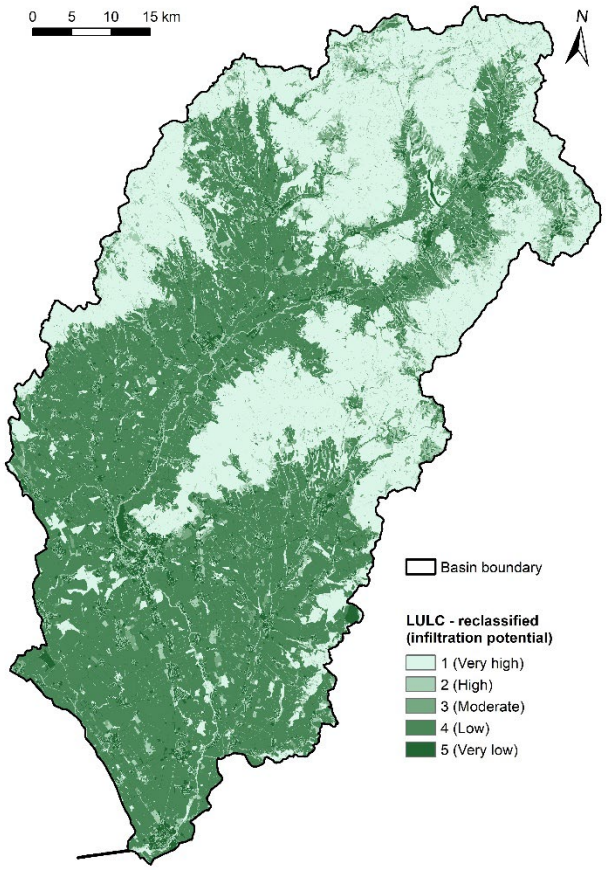

Figure 15. Reclassified LULC in the Nitra River Basin.

3.2. Pluvial flood hazard index

Pluvial floods constitute a significant hazardous event, directly resulting from intense rainfalls that induce rapid surface runoff. Within the scope of the Nitra River Basin, the calculated PFHI serves as the instrumental metric for this purpose, enabling a quantitative spatial assessment of the basin's susceptibility to pluvial flooding.

The map of PFHI was divided into five classes based on Equal interval method (Figure 16). The areas classified under the highest hazard for pluvial flooding are spatially distributed mainly in urban areas or in their proximity. The share of this class on the total basin area is 2.58%. The high hazard class, which represents the dominant category (31.73%), is primarily concentrated in the Podunajská pahorkatina hills or Hornonitrianska kotlina basin.

The moderate hazard class can be found close to high zones. These areas constitute a substantial portion of the basin, accounting for 39.14% of its extent. Conversely, regions characterized by a low hazard for pluvial flooding are predominantly associated with moderate topographic gradients and highly permeable soils, or are situated within the forest complexes. This class represents 18.9% of the basin total area. Finally, the very low hazard class account for 7.65%. It is observed in the higher elevations of the basin, specifically within the mountain ranges of Tribeč, Strážovské vrchy, and Považský Inovec, which occupy the northern, eastern, and western peripheries of the basin.

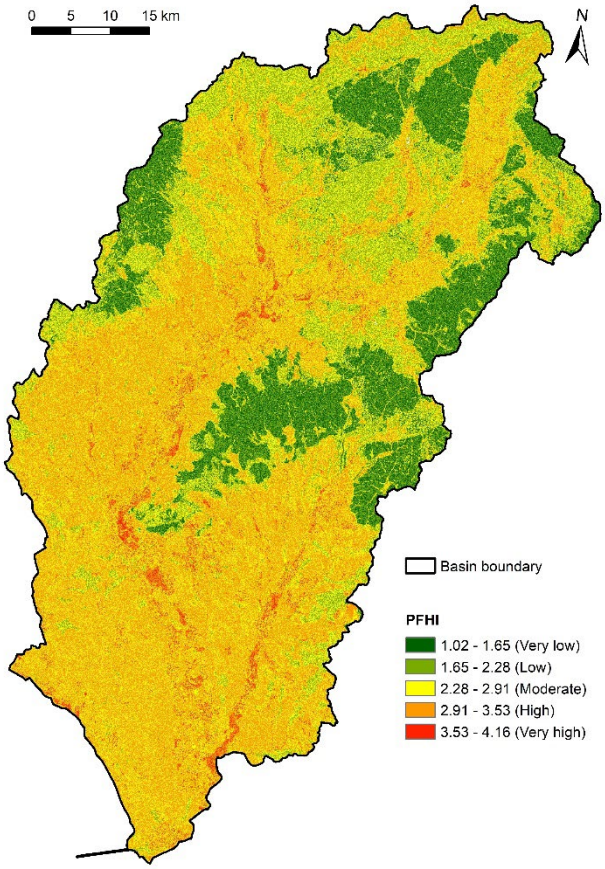

Figure 16. PFHI in the Nitra River Basin.

3.3. Validation of pluvial flood hazard index

As long as reliable validation data for historical pluvial flooding is very scarce, we validated our results on an example of pluvial floods, which occurred in the Nitra Town three times within a single month, in particular, on 10, 16, and 24 June 2024. The cause was intense rainfall that hit the town during cloudbursts. This extreme meteorological phenomenon led to rapid surface runoff and overloading of drainage channels, resulting in pluvial flooding in several parts of the town. The most affected area was the Kynek urban part, where water flooded houses, gardens, and local roads. Photographs reporting the pluvial flood consequences from 16 June 2024 around Nad Hrabinou Street are available at these links: https://www.nitrak.sk/clanky/foto/2506, https://www.nitrak.sk/clanky/foto/2430. Figure 17 shows the comparison of our modeling result (PFHI) in this area and the reconstructed pluvial flood extent

based on the photographs. The total flooded area has 10,654 m^2. The flooded area contains 43.4%, 39.8%, and 16.9% of pixels corresponding to moderate, high, and very high PFHI, respectively. In this area, there are no low or very low PFHI pixels. It means that this area as well as another neighboring streets are highly susceptible to pluvial flooding, which proves the reliability of the calculated PFHI, especially, for this specific area.

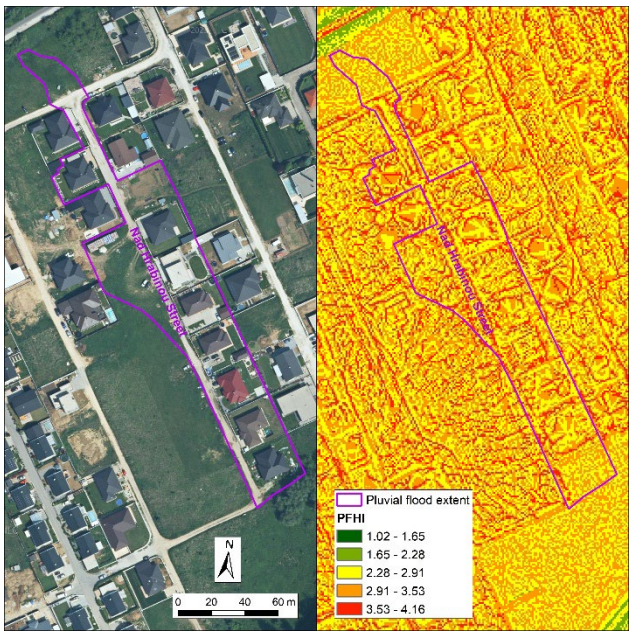

Figure 17. Reconstructed flood extent after pluvial flood from 16 June 2024 and the resulting PFHI values.

4. CONCLUSIONS

The GIS-based method, which was applied in this study, proved its efficiency since the computation and spatial modeling of pluvial flood hazard revealed areas with very high or high potential for pluvial flooding. The validation of the PFHI, though using only one case of observed inundation area during 2024 pluvial flood event, confirmed the reliability of the proposed methodology.

The results of this study can be useful, especially, for Preliminary Flood Risk Assessment (PFRA), which is carried out every six years under the EU Floods Directive (2007), as well as for integrated river basin (flood risk) management and planning. Future research will be directed towards the usage of the physical-geographical indicators and LULC for machine-learning based prediction of pluvial flood hazard in the studied area.

Overall, an attempt was made in this study to contribute to the issue of pluvial flood hazard computation and assessment using straightforward GIS-based methods, which could be simply used and verified in other similar basins. The innovative aspects of this study lie in proposing objective GIS-based approach applicable directly for PFRA at basin scale under the EU Floods Directive (2007). In Slovakia, so far no attempt was made to incorporate similar spatial pluvial flood hazard assessment into PFRA although the nation-wide LiDAR DEM is publicly available from 2017.

Limitations of this study arise, in particular, from data inconsistency used for creating pluvial flood indicators. Half of the indicators (curvature, TWI, and STI) were derived from the LiDAR DEM with 1 m spatial resolution. The LULC indicator was derived from ZBGIS 2023, which is based on orthophotos with 15 cm spatial resolution. The most generalized data used for the computation of the PFHI was lithology, derived from lithological maps at a scale of 1:50,000, and soil texture, which was derived from soil maps at a scale of 1:10,000. Another limitation is in the unavailability of other reliable data for validation of the resulting PFHI. This is a particular problem for larger study areas, as well as for on-site recording of the maximum flood extent, as pluvial floods progress very rapidly.

All in all, the presented results can contribute to optimizing adaptation measures, supporting strategic planning, and increasing the resilience of both landscape and settlements to extreme rainfall events.

Funding

Funded by the EU NextGenerationEU through the Recovery and Resilience Plan for Slovakia under the project No. 09I03-03-V03-00085.

REFERENCES

Allegri, E., Zanetti, M., Torresan, S. & Critto, A., 2024. *Pluvial flood risk assessment for 2021–2050 under climate change scenarios in the Metropolitan City of Venice*. Science of the Total Environment, 914, 169925. https://doi.org/10.1016/j.scitotenv.2024.169925

Bartlett, M.S., Blitterswyk, J.V., Farella, M., Li, J., Smith, C., Parolari, A.J., Krishnamoorthy, L. & Mrad, A. 2025. *Physically Based Dimensionless Features for Pluvial Flood Mapping with Machine Learning*. Water Resources Research, 61(4), e2024WR039086. https://doi.org/10.1029/2024WR039086

Bentivoglio, R., Isufi, E., Jonkman, S.N. & Taormina, R., 2022. *Deep learning methods for flood mapping: a review of existing applications and future research directions*. Hydrology and Earth System Sciences, 26, 4345–4378. https://doi.org/10.5194/hess-26-4345-2022

Beven, K.J., Kirkby, M.J., 1979. *A physically based, variable contributing area model of basin hydrology*.

Hydrological Sciences Bulletin, 24, 43–69.

Blöschl, G., Buttinger-Kreuzhuber, A., Cornel, D., Eisl, J., Hofer, M., Hollaus, M., Horváth, Z., Komma, J., Konev, A., Parajka, J., Pfeifer, N., Reithofer, A., Salinas, J., Valent, P., Výleta, R., Waser, J., Wimmer, M.H. & Stiefelmeyer, H., 2024. *Hyper-resolution flood hazard mapping at the national scale*. Natural Hazards and Earth System Sciences, 24, 2071-2091. https://doi.org/10.5194/nhess-24-2071-2024

Cea, L., Sañudo, E., Montalvo, C., Farfán, J., Puertas, J. & Tamagnone, P. 2025. *Recent advances and future challenges in urban pluvial flood modelling*. Urban Water Journal, 22(2), 149-173.

Costache R., 2019. *Flood susceptibility assessment by using bivariate statistics and machine learning models – a useful tool for flood risk management*. Water Resources Management, 33(9), 3239–3256. https://doi.org/10.1007/s11269-019-02301-z

Costache, R., Pham, Q.B., Corodescu-Roșca, E., Cîmpianu, C., Hong, H., Linh, N.T.T, Fai, C.M., Ahmed, A.N., Vojtek, M., Pandhiani, S.M., Minea, G., Ciobotaru, N., Popa, M.C., Diaconu, D.C. & Pham, B.T., 2020. *Using GIS, Remote Sensing, and Machine Learning to Highlight the Correlation between the Land-Use/Land-Cover Changes and Flash-Flood Potential*. Remote Sensing, 12(9), 1422. https://doi.org/10.3390/rs12091422

Dau, Q.V., Wang, X., Aziz, F., Nawaz, R.A., Pang, T., Mahmood, M.Q. & Fortin, M., 2024. *Pluvial flood modeling for coastal areas under future climate change – A case study for Prince Edward Island, Canada*. Journal of Hydrology, 641, 131769. https://doi.org/10.1016/j.jhydrol.2024.131769

Demek, J., 1972. *Manual of Detailed Geomorphological Mapping*. Academia, Prague.

EU Floods Directive, 2007. *Directive 2007/60/EC of the European Parliament and of the Council of 23 October 2007 on the Assessment and Management of Flood Risks*. https://eur-lex.europa.eu/eli/dir/2007/60/oj/eng

Hrnčiarová, T., 1993. *Hodnotenie potenciálnej zraniteľnosti zásob podzemných vôd pre ekologické plánovanie krajiny* [Assessing the potential vulnerability of groundwater resources for ecological landscape planning]. Životné prostredie, 27, 311–314. (in Slovak)

Intergovernmental Panel on Climate Change (IPCC), 2021. *Climate Change 2021: The Physical Science Basis*. Cambridge University Press. https://www.ipcc.ch/report/ar6/wg1/

Jiang, W., Yu, J., Wang, Q. & Yue, Q., 2022. *Understanding the effects of digital elevation model resolution and building treatment for urban flood modelling*. Journal of Hydrology: Regional Studies, 42, 101122. https://doi.org/10.1016/j.ejrh.2022.101122

Krvavica, N., Šiljeg, A., Horvat, B. & Panđa, L., 2023. *Pluvial Flash Flood Hazard and Risk Mapping in Croatia: Case Study in the Gospić Catchment*. Sustainability, 15(2), 1197. https://doi.org/10.3390/su15021197

Lapin, M., Faško, P., Melo, M., Šťastný, P. & Tomlain, J., 2002. *Climatic regions*. In: Hrnčiarová, T., (Ed.), Landscape atlas of the Slovak Republic. MŽP SR, SAŽP, Bratislava, Banská Bystrica.

Maidment, D.R., 2002. *Arc Hydro: GIS for water resources*. ESRI Press.

Mazúr, E. & Lukniš, M., 1986. *Geomorfologické členenie SSR a ČSSR. Časť Slovensko*. [Geomorphological division of the SSR and ČSSR. Part: Slovakia]. Slovenská kartografia, Bratislava. (in Slovak)

Mediero, L., Soriano, E., Oria, P., Bagli, S., Castellarin, A., Garrote, L. Mazzoli, P., Mysiak, J., Pasetti, S., Persiano, S., Santillán, D. & Schröter, K., 2022. *Pluvial flooding: High-resolution stochastic hazard mapping in urban areas by using fast-processing DEM-based algorithms*. Journal of Hydrology, 608, 127649. https://doi.org/10.1016/j.jhydrol.2022.127649

Moore, I.D., Burch, G.J., 1986. *Physical Basis of the Length-slope Factor in the Universal Soil Loss Equation*. Soil Science Society of America Journal, 50(5), 1294–1298.

Mudashiru, R.B., Sabtu, N., Abustan, I. & Balogun, W. 2021. *Flood hazard mapping methods: A review*. Journal of Hydrology, 603, 126846. https://doi.org/10.1016/j.jhydrol.2021.126846

Papalexiou, S.M. & Montanari, A., 2019. *Global and Regional Increase of Precipitation Extremes Under Global Warming*. Water Resources Research, 55(6), 4901–4914. https://doi.org/10.1029/2018WR024067

Rosenzweig, B.R., McPhillips, L., Chang, H., Cheng, C., Welty, C., Matsler, M., Iwaniec, D. & Davidson, C.I., 2018. *Pluvial flood risk and opportunities for resilience*. WIREs Water, 5(6), e1302. https://doi.org/10.1002/wat2.1302

Rözer, V., Peche, A., Berkhahn, S., Feng, Y., Fuchs, L., Graf, T., Haberlandt, U., Kreibich, H., Sämann, R., Sester, M., Shehu, B., Wahl, J. & Neuweiler, I., 2021. *Impact-based forecasting for pluvial floods*. Earth's Future, 9, e2020EF001851. https://doi.org/10.1029/2020EF001851

Saha, T.K., Pal, S., Talukdar, S., Debanshi, S., Khatun, R., Singha, P. & Mandal, I., 2021. *How far spatial resolution affects the ensemble machine learning based flood susceptibility prediction in data sparse region*. Journal of Environmental Management, 297(1), 113344. https://doi.org/10.1016/j.jenvman.2021.113344

Santos, P.P., Reis, E., Pereira, S. & Santos, M., 2019. *A flood susceptibility model at the national scale based on multicriteria analysis*. Science of the Total Environment, 667, 325–337. https://doi.org/10.1016/j.scitotenv.2019.02.328

Smith, K. & Ward, R., 1998. *Floods: Physical processes and human impacts*. Wiley.

Tanaka, T., Kiyohara, K. & Tachikawa, Y., 2020. *Comparison of fluvial and pluvial flood risk curves in urban cities derived from a large ensemble climate simulation dataset: A case study in Nagoya, Japan*. Journal of Hydrology, 584, 124706. https://doi.org/10.1016/j.jhydrol.2020.124706

Teng, J., Jakeman, A.J., Vaze, J., Croke, B.F.W., Dutta, D. & Kim, S. 2017. *Flood inundation modelling: A review of methods, recent advances and uncertainty analysis*. Environmental Modelling & Software, 90, 201–216. https://doi.org/10.1016/j.envsoft.2017.01.006

Toosi, A.S., Calbimonte, G.H., Nouri, H. & Alaghmand, S., 2019. *River basin-scale flood hazard assessment using a modified multi-criteria decision analysis approach: a case study*. Journal of Hydrology, 574, 660–671. https://doi.org/10.1016/j.jhydrol.2019.04.072

Vojtek, M. & Vojteková, J., 2018. *Flood maps and their potential role in local spatial planning: a case study from Slovakia*. Water Policy, 20(5), 1042–1058. https://doi.org/10.2166/wp.2018.077

Vojtek, M., Vojteková, J. & Pham, Q.B., 2021. *GIS-Based Spatial and Multi-Criteria Assessment of Riverine Flood Potential: A Case Study of the Nitra River Basin, Slovakia*. ISPRS International Journal of Geo-Information, 10(9), 578. https://doi.org/10.3390/ijgi10090578

Vojtek, M., Janizadeh, S. & Vojteková, J., 2022. *Riverine flood potential assessment at municipal level in Slovakia*. Journal of Hydrology: Regional Studies, 46(3), 360–382. https://doi.org/10.1080/03098265.2021.1902958

Vojtek, M., Vojteková, J., De Luca, D.L. & Petroselli, A., 2023a. *Combined basin-scale and decentralized flood risk assessment: a methodological approach for preliminary flood risk assessment*. Hydrological Sciences Journal, 63(3), 355–378. https://doi.org/10.1080/02626667.2022.2157279

Vojtek, M., Janizadeh, S., & Vojteková, J., 2023b. *Riverine flood potential assessment using metaheuristic hybrid machine learning algorithms*. Journal of Flood Risk Management, 16(3), e12905. https://doi.org/10.1111/jfr3.12905

Vojtek, M., Moradi, S., De Luca D.L., Petroselli, A. & Vojteková, J., 2024. *Fluvial and pluvial flood hazard mapping: combining basin and municipal scale assessment*. Geomatics, Natural Hazards and Risk, 15(1), 2432377. https://doi.org/10.1080/19475705.2024.2432377

Vojteková, J. & Vojtek, M., 2019. *GIS-Based Landscape Stability Analysis: A Comparison of Overlay Method and Fuzzy Model for the Case Study in Slovakia*. The Professional Geographer, 71(4), 631–644. https://doi.org/10.1080/00330124.2019.1611454

Welten, S., Holt, A., Weber, S., Klopries, E.M., Schüttrumpf, H. & Decker, S., 2024. *Generation of harmonised pluvial flood hazard maps through decentralised analytics*. Journal of Hydroinformatics, 26(2), 534–548. https://doi.org/10.2166/hydro.2024.257

Yu, J., Li, Y, Huang, X. & Ye, X., 2025. *Data quality and uncertainty issues in flood prediction: a systematic review*. International Journal of Digital Earth, 18(1), 2495738. https://doi.org/10.1080/17538947.2025.2495738

Zoppou, C., 2001. *Review of urban stormwater models*. Environmental Modelling & Software, 16(3), 195–231. https://doi.org/10.1016/S1364-8152(00)00084-0

Received: 05. 12. 2025
Revised: 15. 01. 2026
Accepted: 17. 01. 2026
Published online: 24. 01. 2026